Nuclear Instruments and Methods in Physics Research A 844 (2017) 14–18

Contents lists available at ScienceDirect

Nuclear Instruments and Methods in Physics Research A

journal homepage: www.elsevier.com/locate/nima

A simple decay-spectroscopy station at CRIS-ISOLDE

K.M. Lynch[a,b,*], T.E. Cocolios[a,c], N. Althubiti[c], G.J. Farooq-Smith[a,c], W. Gins[a], A.J. Smith[c]

[a] KU Leuwen, Instituut voor Kern, en Stralingsfysica, BE-3001 Leuwen, Belgium
[b] EP Department, CERN, CH-1211 Geneva 23, Switzerland
[c] School of Physics and Astronomy, The University of Manchester, Manchester M13 9PL, United Kingdom

ARTICLE INFO

Keywords:
Alpha-decay spectroscopy
Gamma-ray spectroscopy
Laser-assisted nuclear decay spectroscopy
RIB

ABSTRACT

A new decay-spectroscopy station (DSS2.0) has been designed by the CRIS collaboration for use at the radioactive ion beam facility, ISOLDE. With the design optimised for both charged-particle and γ-ray detection, the DDS2.0 allows high-efficiency decay spectroscopy to be performed. The DSS2.0 complements the existing decay-spectroscopy system at the CRIS experiment, and together provide the ability to perform laser-assisted nuclear decay spectroscopy on both ground state and long-lived isomeric species. This paper describes the new decay-spectroscopy station and presents the characterisation studies that have recently been performed.

1. Introduction

The CERN-ISOLDE facility [1,2] provides beams of radioactive isotopes, ranging from $_{2}$He to $_{92}$U, to a variety of experimental setups. Many of these experiments perform nuclear decay spectroscopy, either as a direct measurement or for identification of the isotope of interest.

The collinear resonance ionization spectroscopy (CRIS) experiment [3–5] at ISOLDE is a laser spectroscopy setup with the ability to perform nuclear decay spectroscopy in parallel. By combining the high resolution of collinear laser spectroscopy with the high efficiency of resonance ionization and ion detection [6], high-resolution, high-sensitivity studies of hyperfine structures and isotope shifts can be performed [7–9]. For hyperfine-structure studies, the frequency of the laser is scanned and the ion rate is measured as a function of applied frequency. With the added capability of studying the radioactive decay of the isotope under investigation, the CRIS experiment has the ability to identify complex hyperfine structures, and perform dedicated laser-assisted nuclear decay spectroscopy.

When an isotope has a long-lived isomer ($T_{1/2} \geq 5$ ms), its hyperfine structure and isomer shift can be studied alongside the ground state. In such cases, when each state's hyperfine structure cannot be identified with the usual methods of ion-counting (resonance peak location, separation, intensity, etc.), additional selection is necessary. Identification of the resonances can be achieved by studying the nuclear decay of the isotope of interest [10]. In a recent series of campaigns, the isomers in ^{202,204,206,214}Fr were studied via their characteristic α-particle energies [11–13], and the state observed in ^{218}Fr via its characteristic half-life [14].

Conversely, the high resolution of the CRIS experiment can be used to separate isotopes from isobaric contamination, and even isomers from each other. This was also successfully demonstrated and allowed the first measurement of the branching ratios in the decay of $^{204\ m2}$Fr [11] and $^{206\ m2}$Fr [12].

These campaigns were performed using the decay spectroscopy station DSS [15], which has been tailored to maintain the high vacuum required by the CRIS experiment, at the expense of γ-ray detection efficiency (<0.01% at 1 MeV in the aforementioned campaigns). Moreover, the limited number of implantation sites in the DSS (of 8 carbon foils) prevents the complete removal of long-lived activity, as would be achieved with a tape system.

In this article, we present the design of a new decay spectroscopy station, with the primary focus of increased γ-ray detection efficiency and versatility, alongside its offline-characterisation studies.

2. DSS2.0 Design

The new decay-spectroscopy station (DSS2.0) consists of a rectangular, aluminium chamber (dimensions: 10 × 10 × 25 cm) that can be mounted onto a DN100 vacuum flange. Three of the four side panels are braised, thin (2 mm) aluminium walls for minimising γ-ray absorption. The fourth panel is a base plate on which the sample holder, in-vacuum detectors, and associated connectors are placed. The back panel is a removable aluminium plate, which allows the future installation of a beryllium window or ancillary detectors, depending upon the physics case of interest. Two silicon detectors are mounted on the base plate for charged-particle spectroscopy, either side of an implantation site. A stainless steel mount holding two carbon foils and an insulated copper plate (used as a Faraday cup) is typically used as

* Corresponding author at: EP Department, CERN, CH-1211 Geneva 23, Switzerland.
E-mail address: kara.marie.lynch@cern.ch (K.M. Lynch).

http://dx.doi.org/10.1016/j.nima.2016.11.024
Received 20 June 2016; Received in revised form 25 October 2016; Accepted 5 November 2016
Available online 12 November 2016

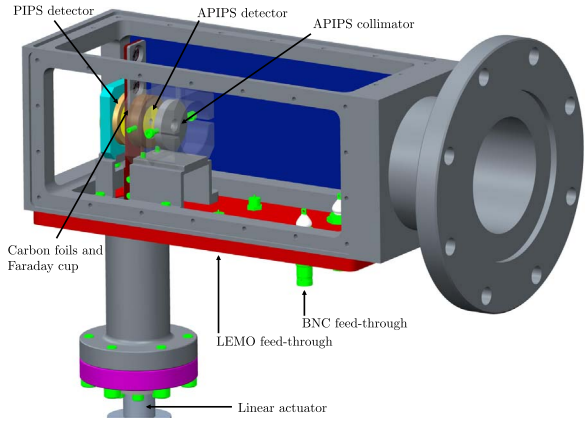

Fig. 1. 3D representation of the DSS2.0 chamber.

the implantation site. A Kapton® shielded wire is soldered onto the copper plate and connected to a LEMO® connection, allowing an electrical current to be measured and the plate to be used as a beam-monitoring device. The Faraday cup is electrically insulated from the surrounding stainless steel by PEEK® rings either side of the copper plate. Exchange of the mount for an aluminised Mylar® tape is possible, with no modification to the base plate configuration necessary (see Fig. 1).

2.1. For α-decay spectroscopy

Two Canberra PIPS detectors are installed in the DSS2.0 for charged-particle detection, either side of a stainless steel mount containing two carbon foils and a Faraday cup. An annular PIPS (APIPS) detector (model: BKANPD 300-18 RM, thickness: 300 μm, active area: 300 mm^2, hole diameter: 4 mm) is placed in front of the carbon-foil holder, and a standard PIPS detector (model: BKA 300-17 AM, thickness: 300 μm, active area: 300 mm^2) is installed behind. The detectors are connected to Canberra preamplifiers (model: 2003BT) via custom-made Microdot cables and BNC feedthroughs. Installed in the stainless-steel mount (dimensions: 12 × 10 × 2 mm^3) are two carbon foils (thickness: 20(1)μg cm^{-2} or 90 nm, diameter: 10 mm [16]) and a copper Faraday cup (thickness: 0.5 mm, diameter: 10 mm). Each carbon foil is attached to one side of a 1-mm thick copper o-ring, to aid manipulation. Each carbon-foil assembly is inserted into a circular groove in the stainless-steel mount, to fix in place. This mount is attached to a Kurt J. Lesker linear actuator (model: KLPDBAP) that allows its position to be varied to place either the carbon foils or Faraday cup in between the PIPS detectors (see Fig. 2).

The Faraday cup is used for tuning the beam through the aperture of the annular PIPS detector. For nuclear decay measurements, the radioactive ion beam is focused through the aperture of the annular PIPS detector and implanted into one of the carbon foils. Radioactive decay products (α or β particles, fission fragments, conversion electrons) emitted from the implanted isotopes are measured with the surrounding PIPS detectors.

GEANT4 [17] simulations were performed to determine the most appropriate orientation of the carbon foil and the optimal position of the annular PIPS detector with respect to the carbon foil holder (see Fig. 3). The α-particle source was spread uniformly across the carbon foil in the area that may be reached through the 4 mm hole in the APIPS detector. The distance between the PIPS detectors and the stainless steel mount was varied, and the position of the carbon foil flipped between facing closest to the annular PIPS (position 0) or the standard PIPS (position 1), see Fig. 4. This was achieved by over-turning the copper o-ring that the carbon foil was attached to, inside the stainless steel mount. The PIPS detector is placed in close geometry to the carbon foil holder (between 0.4 and 1.6 mm), represented by the

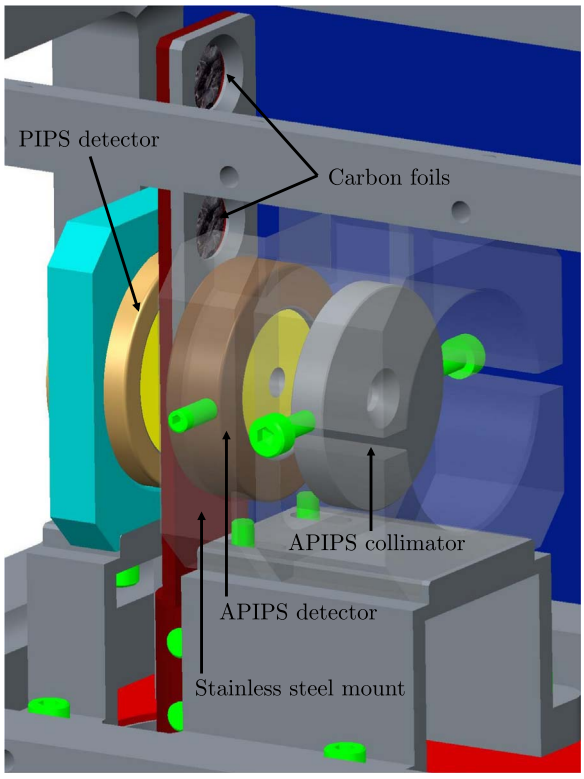

Fig. 2. Detailed view of the implantation site and PIPS detectors.

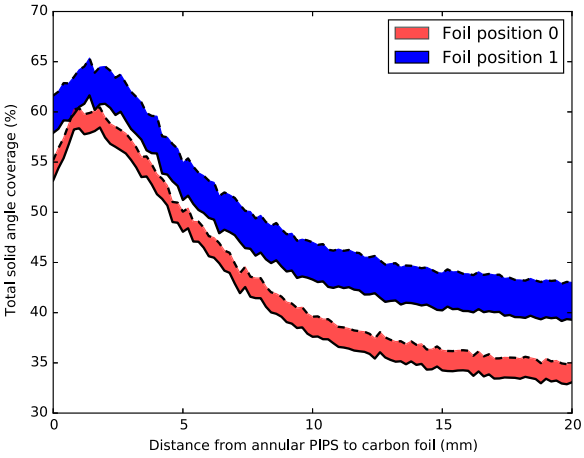

Fig. 3. Solid angle coverage of the PIPS detectors as a function of distance of the annular PIPS detector to the carbon foil. The orientation of the foil is closest to the annular PIPS detector in position 0 (Fig. 4a) and the standard PIPS detector in position 1 (Fig. 4b). The width of the curve represents the tolerance of the PIPS position in the detector mount: between 0.4 mm (dashed line) and 1.6 mm (solid line).

width of the curves in Fig. 3. It was concluded that the highest efficiency is obtained with the foil in position 1, facing closest to the standard PIPS, which is positioned at 0.4 mm from the carbon foil holder. The annular PIPS detector is mounted at an optimal distance of 1.5 mm from the carbon foil holder, resulting in an expected total solid angle of 65%.

SRIM [18] simulations were performed to investigate the depth of implantation of the ion beam into the carbon foil, the energy loss of the α particle upon exiting the foil, and the recoil of the daughter nucleus. A normally incident beam of $^{206}Fr^{+}$ at 40 keV was chosen as a case study. The implantation profile can be seen in Fig. 5 (top). The implantation depth was found to be 21 nm, with a full width at half maximum of 7 nm.

This initial distribution of ^{206}Fr ions (21 nm deep in the carbon foil,

(a) Foil position 0 (b) Foil position 1

Fig. 4. Schematic of the carbon foil (yellow), attached to the copper o-ring (dark yellow), inside the stainless steel mount (dark red/silver). Two configurations are possible: the foil (a) closest to the annular PIPS detector or (b) closest to the standard PIPS detector. The highest efficiency is found in configuration (b). The thickness of the carbon foil is exaggerated for viewing purposes. (For interpretation of the references to color in this figure caption, the reader is referred to the web version of this paper.)

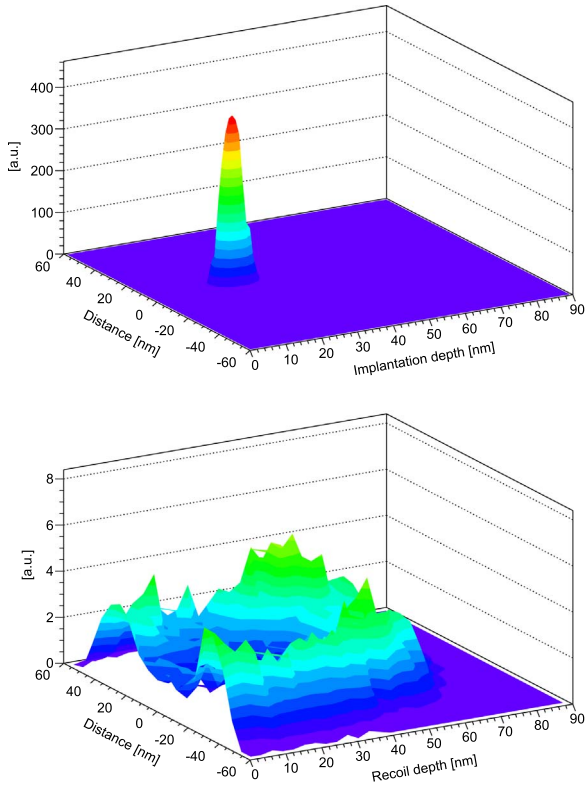

Fig. 5. (Top) Implantation profile of a beam of $^{206}Fr^{+}$ at 40 keV onto the DSS carbon foil. (Bottom) Recoil profile of ^{202}At from α decay at 6792 keV within the DSS carbon foil.

7 nm FWHM) was used as a starting sample for the α decay. An isotropic decay pattern was randomly generated from this sample, with α particles of energy 6792 keV. The trajectories of these α particles were then simulated through the carbon foil and extrapolated in order to determine the fraction of particles reaching the PIPS detectors. A total efficiency of 65% is found, in agreement with the GEANT4

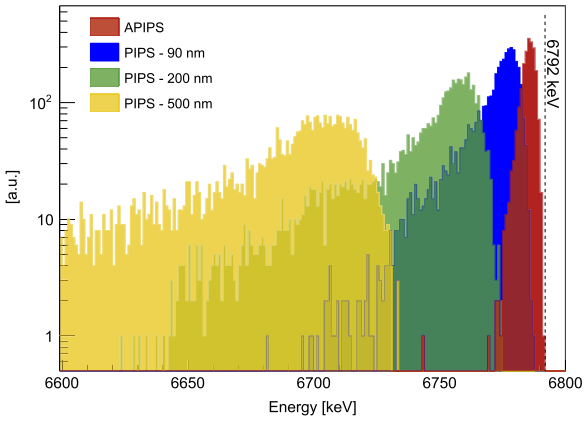

Fig. 6. Simulated α-decay energy spectra of ^{206}Fr in the carbon foil. The dotted line marks the α-particle initial energy of 6792 keV. The displacement and low-energy tails are due to the α particle energy loss through the carbon foil for thicknesses of 90 nm, 200 nm and 500 nm.

simulations.

The degraded α-particle energies are plotted in Fig. 6. Four α-particle energy spectra are shown: one for the APIPS detector and three for the PIPS detector when the 40-keV ^{206}Fr ions are implanted into a carbon foil of 90 nm, 200 nm and 500 nm, respectively. For each spectrum, the 6792-keV α-particle energy peak is displaced to a lower energy. Additionally, a low-energy tail, corresponding to the particles traveling with a large angle through the carbon foil, is present, which becomes more pronounced for thicker carbon foils. The line profiles were fit with a Crystal Ball function, which combines a Gaussian with a power-law low-energy tail [19,20], to reproduce the energy loss effects. For an intrinsic α-particle energy resolution of 30 keV, the energy straggling contributes less than 1 keV to the FWHM for the APIPS detector. For the PIPS detector, the degradation of the α-particle energy contributes 1 keV, 2 keV, and 8 keV to the energy resolution, for carbon foil thickness of 90 nm, 200 nm and 500 nm, respectively.

The distribution of the recoiling daughter nuclei ^{202}At (after emission of the 6792-keV α particle) were also investigated with SRIM, using the same distribution as that of the α-particle study. The recoil energy is 135 keV, which is greater than the 40 keV implantation energy, and a fraction of the recoils are accordingly ejected from the carbon foil. This effect was already identified, and accounted for, in studies with similar setups [21]. The distribution of the recoils remaining in the carbon foil can be seen in Fig. 5 (Bottom). The fraction of recoils remaining in the foil is 71%. Of the ejected recoils, a fraction is deposited on the surface of the annular silicon detector, amounting to 10% of all the recoils.

The thickness of the carbon foil is a compromise between beam-implantation depth, α-particle energy straggling and ease of use. At 90 nm, the carbon foils are thick enough to stop not only the incoming ion beam (with a nominal energy of 30 or 40 keV), but at least one α-decay particle recoil. Conversely, the foils are thin enough to let the emitted α particle through, to be detected by the PIPS detector, with minimal α-particle energy straggling.

2.2. For β-decay spectroscopy

When performing β-decay spectroscopy, the spectra become highly contaminated in time as isobars and daughter nuclei with longer half-lives than the beam of interest accumulate at the measurement point. A traditional approach to minimise the impact of this contamination is to regularly remove the sample until it is completely out of sight of the detectors. The stainless steel mount with only two carbon-foil implantation sites (presented for α-decay spectroscopy) is therefore not appropriate, and a different geometry is required.

For a dedicated β-decay spectroscopy experiment, it is possible to

remove the linear-actuator assembly from the chamber and replace with the ISOLTRAP tape system [22,23]. The Mylar® tape system allows the complete removal of accumulated β-emitting radioactivity. With over 1 km of tape installed in the system, there are more than 1000 individual implantation sites available before the tape is reused. Additionally, the ISOLTRAP tape system is equipped with a secondary charged-particle and γ-ray detection point where the removed activity can be further studied.

2.3. For γ-ray spectroscopy

Up to three germanium detectors can be placed around the DSS2.0 chamber to detect the x and γ rays emitted from the implantation site. The back panel can also be changed for a beryllium window for the study of low-energy x and γ rays. In this configuration, the PIPS detector behind the implantation point is removed. This port may also be used to insert an ancillary detector, e.g. silicon lithium drifted detector (SiLi) for the high-resolution study of conversion electrons.

2.4. Beam tuning

For stable-beam tuning, the ion beam is focused through the 4 mm aperture of the annular PIPS detector and impinged upon the Faraday cup. A collimator with a 4 mm aperture is placed in front of the annular detector to avoid implanting beam directly onto the detector.

Additionally, the current of beam impinging upon the collimator upstream of the annular detector allows the fraction of the beam that does not pass within the aperture to be measured. A second electrical connection is made with Kapton® shielded wire from the steel collimator to another LEMO® connection. Highest transmission is achieved by maximising the signal on the Faraday cup and minimising it on the collimator.

2.5. Data acquisition

The data acquisition system used for the DSS2.0 characterisation comprises of a VME-based 8-channel digitiser (CAEN V1724) with a sampling rate of 100 MHz. Each detector is connected to a channel and the pre-amplified signal is analysed via on-board digital pulse processing for pulse height analysis (DPP-PHA). Each event is also attributed a time stamp for the post-processing of the time behavior of the signal and reconstructing coincidences between different detectors. The parameters for the DPP-PHA are tuned for each detector independently to offer the highest performance.

The data is acquired using Daresbury's Multi Instance Data Acquisition System (MIDAS) [24] and analyzed with a bespoke conversion and analysis code [25].

3. Offline characterisation

The performance of the DSS2.0 has been characterised off-line using sources of long-lived radio-isotopes.

3.1. α-Decay spectroscopy

The performance characteristics to detect α-decay were studied with an α source (4α) containing 1 kBq of four radioactive isotopes (^{148}Gd, ^{239}Pu, ^{241}Am, and ^{244}Cm) on a copper disk. Since the α particles can only be emitted in one direction, only the PIPS detector was installed in the chamber. An energy resolution of 30 keV at 5.5 MeV was achieved for the PIPS detector. This is sufficient to resolve the α-particle energies of the isotopes of interest in future studies. No absolute efficiency measurements could be made however, due to the geometry of the 4α source and the difficulty placing it in the correct position of the carbon foil.

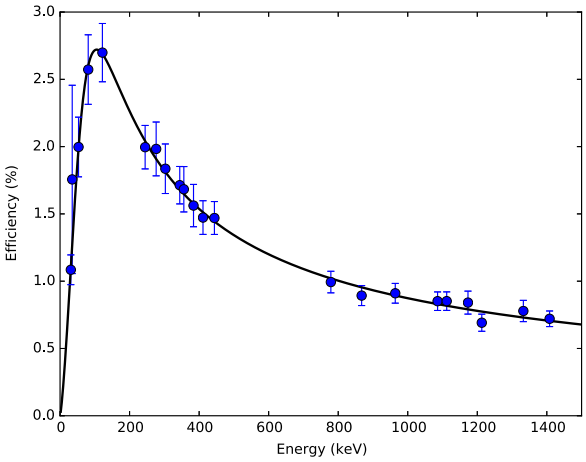

Fig. 7. γ-ray efficiency curve for a single-crystal Canberra XtRa germanium detector, measured using ^{60}Co (723 Bq), ^{133}Ba (11.6 kBq) and ^{152}Eu (16.3 kBq).

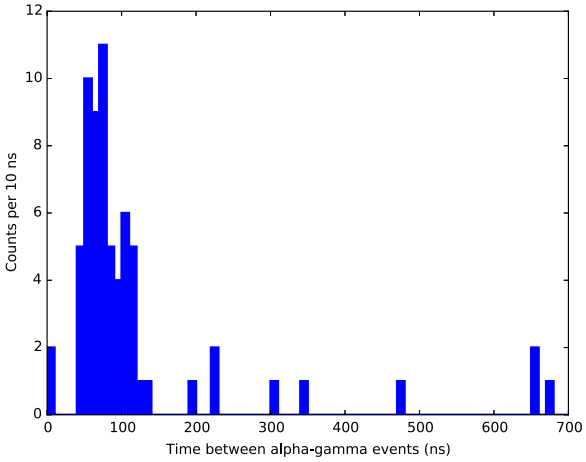

Fig. 8. Time difference spectrum between the silicon and germanium detectors using the 4α source(1 kBq of ^{148}Gd, ^{239}Pu, ^{241}Am, ^{244}Cm). A prompt peak at $\Delta t < 150$ ns identifies the coincident events.

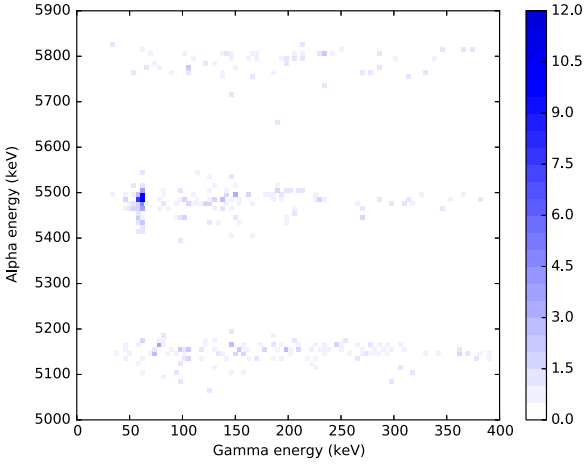

Fig. 9. Random-subtracted coincidence matrix between the silicon and germanium detectors using the 4α source(1 kBq of ^{148}Gd, ^{239}Pu, ^{241}Am, ^{244}Cm). The high concentration of points corresponds to the α-particle emission (5486 keV) of ^{241}Am, followed by the 60-keV γ-ray decay.

3.2. γ-Ray spectroscopy

The γ-decay performances were studied with single-isotope sources of ^{60}Co, ^{133}Ba, and ^{152}Eu, with respective activities 723 Bq, 11.6 kBq,

and 16.3 kBq. A Canberra extended range (XtRa) coaxial germanium detector (model: GX6020) was installed directly outside the chamber to record the emitted γ rays. An energy resolution of 3.5 keV at 1 MeV was interpolated from a fit of FWHM with respect to γ-ray energy.

Fig. 7 shows the photo-peak γ-ray detection efficiency of the Canberra XtRa germanium detector. A peak efficiency of 2.7% at 100 keV compares favourably to the detection efficiency of the original DSS chamber of 0.007% [15].

The benefit of the increased γ-ray detection efficiency is illustrated with the example of the 531 keV γ-ray decay of $^{206\ m2}$Fr, assuming standard ISOLDE yields. At this energy, the original DSS has a γ-ray detection efficiency of 0.005%, resulting in a necessary measurement time of 1 h 57 min for an integrated number of 10,000 γ-ray events. For the same number of integrated counts, the DSS2.0, with a detection efficiency of 1.3% at 531 keV, would take only 27 s

3.3. Charged-particle-γ coincidences

Using the 4α source, it was possible to study the coincidences between α decays and γ rays using the decay of ^{241}Am. The time difference between the silicon and germanium detector signals is shown in Fig. 8. A prompt peak is identified for time differences of $\Delta t < 150$ ns, followed by random events.

Using the timing selection criterion of $\Delta t < 150$ ns, a two-dimensional matrix was created, showing the energy dependence of the events according to both the α particle and the γ ray (see Fig. 9). From this coincidence matrix, a time component (10% of events that occurred in the window $150\ \text{ns} < \Delta t < 1650\ \text{ns}$) was subtracted to account for random events. A high concentration of points is identified around $E_\alpha = 5500$ keV and $E_\gamma = 50$ keV, corresponding to the α-particle emission (5486 keV) of ^{241}Am, followed by the 60-keV γ-ray decay [26]. The efficiency of the $\alpha - \gamma$-coincidences were found to be self-consistent with the measured efficiency of α-particle and γ-ray detection.

4. Summary

A new decay spectroscopy station, named DSS2.0, has been designed and built for the CRIS experiment at ISOLDE. Its main purpose is the study of charged-particle and γ decays at CRIS and is therefore made in a compact geometry with thin aluminium walls.

The DSS2.0 has been characterised offline. Radioactive-decay energy spectra have been acquired with long-lived radioactive sources for the silicon PIPS and germanium detectors, and coincidences between the detectors investigated. The resolution and efficiency of the PIPS detectors are similar to the original decay spectroscopy station at CRIS. The γ-ray detection efficiency is nearly a factor of 400 better than the DSS. The performance of the DSS2.0 is found to be appropriate for the intended future studies.

While the DSS2.0 was initially intended for performing laser-assisted nuclear decay spectroscopy at the CRIS experiment, the small size and portable nature of the device allows its installation at several experimental setups at ISOLDE. A commissioning experiment studying the α decay of the light mercury isotopes has been performed with the DSS2.0 at the GLM beamline at ISOLDE [27]. The chamber has also been utilised during an ISOLTRAP experiment studying the polonium isotopes. The DSS2.0 was installed after the ISOLTRAP multi-reflection time-of-flight mass separator (MR-TOF-MS) [28,29], where it was used to measure the ratio of ground- to isomeric-state in the odd-A neutron-deficient polonium beams.

Acknowledgements

The authors extend their thanks to the GSI target lab for producing the carbon foils, The University of Manchester machine shop for their work, and the ISOLTRAP Collaboration for the use of their tape system. This work was funded by the STFC Consolidated Grant No. ST/F012071/1, STFC Continuation Grant No. ST/J000159/1, STFC Ernest Rutherford Grant No. ST/L002868/1, The Royal Society of London, FWO-Vlaanderen (Belgium), GOA/2010/010 (BOF-KULeuven), and by the IUAP-Belgian State Belgian Science Policy (BRIX network P7/12). K. M. L. was supported by the FWO Pegasus Marie Curie Fellowship No. 267216, T. E. C. was supported by the STFC Ernest Rutherford Fellowship No. ST/J004189/1, and N. A. was supported by a scholarship from Al-jouf University.

References

[1] E. Kugler, The ISOLDE facility, Hyperfine Inter. 129 (2000) 23–42.
[2] B. Jonson, A. Richter, More than three decades of ISOLDE physics, Hyperfine Inter. 129 (2000) 1.
[3] T.J. Procter, et al., Development of the CRIS (Collinear Resonant Ionisation Spectroscopy) beam line, J. Phys. Conf. Ser. 381 (2012) 012070.
[4] K.T. Flanagan, et al., Collinear resonance ionization spectroscopy of neutron-deficient francium isotopes, Phys. Rev. Lett. 111 (2013) 212501.
[5] T.E. Cocolios, et al., High-resolution laser spectroscopy with the collinear resonance ionisation spectroscopy (CRIS)experiment at CERN-ISOLDE, Nucl. Instrum. Methods Phys. Res. B 376 (2016) 284–287.
[6] Y.A. Kudriavtsev, V.S. Letokhoov, Laser method of highly selective detection of rare radioactive isotopes through multistep photoionization of accelerated atoms, Appl. Phys. B 29 (1982) 219.
[7] B. Cheal, K.T. Flanagan, Progress in laser spectroscopy at radioactive ion beam facilities, J. Phys. G. 37 (2010) 113101.
[8] K. Blaum, J. Dilling, W. Nörterhäuser, Precision atomic physics techniques for nuclear physics with radioactive beams, Phys. Scr. T152 (2013) 014017.
[9] P. Campbell, I.D. Moore, M.R. Pearson, Laser spectroscopy for nuclear structure physics, Progr. Part. Nucl. Phys. 86 (2015) 127–180.
[10] K.M. Lynch, et al., CRIS: a new method in isomeric beam production, Eur. Phys. J. Web Conf. 63 (2013) 01007.
[11] K.M. Lynch, et al., Decay-assisted laser spectroscopy of neutron-deficient francium, Phys. Rev. X 4 (2014) 011055.
[12] K.M. Lynch, et al., Combined high-resolution laser spectroscopy and nuclear decay spectroscopy for the study of the low-lying states in ^{206}Fr, ^{202}At, and ^{198}Bi, Phys. Rev. C. 93 (2016) 014319.
[13] G.J. Farooq-Smith, et al., Laser and decay spectroscopy of the short-lived isotope ^{214}Fr in the vicinity of the N =126 shell closure, Phys. Rev. C. 94 (2016) 054305. http://dx.doi.org/10.1103/PhysRevC.94.054305.
[14] I. Budinčević, et al., Laser spectroscopy of francium isotopes at the borders of the region of reflection asymmetry, Phys. Rev. C. 90 (2014) 014317.
[15] M.M. Rajabali, K.M. Lynch, T.E. Cocolios, et al., A dedicated decay-spectroscopy station for the collinear resonant ionization experiment at ISOLDE, Nucl. Instrum. Methods Phys. Res. A 707 (2013) 35–39.
[16] B. Lommel, W. Hartmann, B. Kindler, J. Klemm, J. Steiner, Preparation of self-supporting carbon thin films, Nucl. Instrum. Methods Phys. Res. A 480 (2002) 199–203.
[17] S. Agostinelli, et al., GEANT4-a simulation toolkit, Nucl. Instrum. Methods Phys. Res. A 506 (2003) 250–303.
[18] J.F. Ziegler, M.D. Ziegler, J.P. Biersack, Srim—the stopping and range of ions in matter (2010), Nucl. Instrum. Methods Phys. Res. B 268 (2010) 1818–1823.
[19] T. Skwarnicki, A study of the radiative cascade transitions between the upsilon-prime and upsilon resonances, (Ph.D. thesis), Institute of Nuclear Physics, Cracow, Poland, DESY-F31-86-02 (1986).
[20] J. Gaiser, Charmonium Spectroscopy from Radiative Decays of the J/ψ and ψ', (Ph. D. thesis), Stanford University, Stanford, California, USA, SLAC-0255 (1982).
[21] H. De Witte, et al., Alpha-decay of neutron-deficient ^{200}Fr and heavier neighbours, Eur. Phys. J. A 23 (2005) 243–247.
[22] M. Kowalska, et al., Trap-assisted decay spectroscopy with ISOLTRAP, Nucl. Instrum. Meth. Phys. Res. A 689 (2012) 102–107.
[23] J. Stanja, et al., Mass spectrometry and decay spectroscopy of isomers across the Z =82 shell closure, Phys. Rev. C. 88 (2013) 054304.
[24] D. Laff, V. Pucknell, Multi-Instance Data Acquisition System, ⟨http://npg.dl.ac.uk/MIDAS/⟩(2016).
[25] K.M. Lynch, DSS Data Fitter, GitHub repository, ⟨https://github.com/karamarielynch/dss-df⟩(2016).
[26] M.S. Basunia, Nucl. Data Sheet 107 (2006) 3323.
[27] T. Day Goodacre, et al., Blurring the boundaries between ion sources: the application of the RILIS inside a FEBIAD type ion source at ISOLDE, Nucl. Instrum. Meth. Phys. Res. B 376 (2016) 39–45.
[28] R.N. Wolf, et al., On-line separation of short-lived nuclei by a multi-reflection time-of- flight device, Nucl. Instrum. Methods Phys. Res. A 686 (2013) 82–90.
[29] R.N. Wolf, et al., ISOLTRAPs multi-reflection time-of-flight mass separator/spectrometer, Int. J. Mass Spectrom. 349–350 (2013) 123–133.